Inorganic Chemistry

Article

pubs.acs.org/IC

Ruthenium(II) Tris(2,2′-bipyridine)-Templated Zinc(II) 1,3,5-Tris(4-carboxyphenyl)benzene Metal Organic Frameworks: Structural Characterization and Photophysical Properties

Christi L. Whittington, Lukasz Wojtas, and Randy W. Larsen*

Department of Chemistry, University of South Florida, 4202 East Fowler Avenue, Tampa, Florida 33620, United States

Supporting Information

ABSTRACT: The ability to confine photoactive catalysts within metal organic framework (MOF) materials affords the opportunity to expand the functional diversity of these materials into solar-based applications. Here, two new Ru(II) tris(2,2′-bipyridine) (RuBpy)-based photoactive materials derived from reactions between Zn(II) ions and 1,3,5-tris(4-carboxyphenyl)benzene and templated by the presence of RuBpy (RWLC-1 and RWLC-2) are described with regard to structure and RuBpy photophysics. RuBpy cations have been successfully encapsulated within the cavities (RWLC-1) and channels (RWLC-2) of the new negatively charged frameworks, both of which are synthesized simultaneously in a single reaction vial. Single-crystal X-ray diffraction studies allowed for determination of the RuBpy position within crystal voids. RuBpy encapsulated in each of the two new MOFs exhibits biphasic triplet metal to ligand charge transfer (^{3}MLCT) emission decay lifetimes ($\tau_{RWLC\text{-}1\text{-}fast}$ = 237 ns, $\tau_{RWLC\text{-}1\text{-}slow}$ = 1.60 μs, $\tau_{RWLC\text{-}2\text{-}fast}$ = 171 ns, and $\tau_{RWLC\text{-}2\text{-}slow}$ = 797 ns at 25 °C) consistent with two populations of RuBpy complexes, one being encapsulated in highly space-restricted cavities giving rise to a longer ^{3}MLCT lifetime, while the second is encapsulation within a larger nonperiodic pore or defect with a coencapsulated quencher giving rise to short emission lifetimes. Taken together, these results represent examples of the templating ability of RuBpy to produce novel materials with distinct photophysical environments of the encapsulated guests.

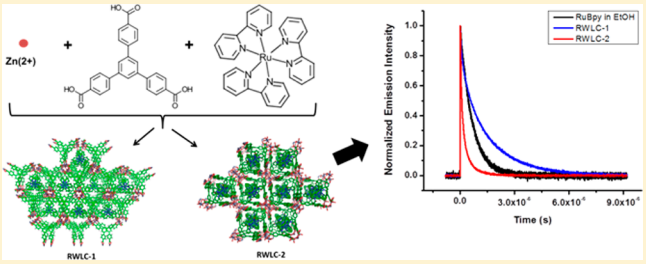

INTRODUCTION

Metal organic frameworks (MOFs) are porous solid-state materials composed of organic linkers and metal coordination complexes (molecular building blocks or MBBs). The key advantages associated with this type of material include the fact that the geometry of the MBB can be "tuned", the organic ligand can be modified to provide functional diversity, both the MBB and the ligand are modular, allowing for a wide range of structures, and the scale of the structure can be tuned from nanoporous to mesoporous.[1−6] These factors allow for extraordinary versatility in structure/function not available to existing porous materials. With regard to structural diversity, these materials extend from discrete nanoscale faceted polyhedra to large porous extended networks.[7] Extended porous networks with regular nanoscale cavities are of particular importance for catalyst development since these materials can accommodate a wide variety of guest molecules including various porphyrin macrocycles,[8−11] polyoxymetalates,[12−17] and metallo-bipyridine clusters.[18−22]

Porous MOFs offer great potential for photocatalytic applications. Photocatalytic MOFs have been developed in which Keggin-type polyoxymetalate clusters have been encapsulated within an HKUST-1 framework,[12,13] free base and metalloporphyrins encapsulated within both rhoZMOF and HKUST-1 framework,[8−10] and RuBpy encapsulated in pillared 2-D sheet materials, a Zn(II) trimesic acid-based MOF (USF2),[18,19] and oxalate−metal frameworks.[20,23−27] In the case of encapsulated photocatalytic materials, the target reactants diffuse through available channels and cavities within the MOF, encounter the photoexcited catalyst, undergo photochemical transformation, and subsequently diffuse back through the pores/channels eventually exiting the material. This type of photocatalytic MOF offers a number of advantages including the fact that a wide array of existing photocatalysts can be exploited, reactant molecules must enter the pores of the MOF in order to react with the photocatalyst, thus allowing for selective chemistry to take place at specific sites within the MOF, and the large library of existing MOFs can be targeted with little need for new MOF designs or exotic ligands.

Ruthenium(II) polypyridyl complexes are of specific interest as guests in development of photocatalytic MOFs due to the fact that the excited states of Ru(II)(L)$_3$ complexes exhibit favorable reduction/oxidation potentials in the excited state as well as relatively long lifetimes (allowing for greater excited-state reactivity), and the complexes have excellent photostability.[28] In addition, a wide array of functionalized bipyridine ligands is available which can be utilized to further tune the excited-state properties of the Ru(II)(L)$_3$-type complexes. The RuBpy complex has been previously encapsulated in numerous

Received: July 25, 2013
Published: December 13, 2013

   dx.doi.org/10.1021/ic402614w | Inorg. Chem. 2014, 53, 160−166

solid-state materials including inorganic zeolites,[29−32] zirconium phosphate layered materials,[33,34] sol−gel matrices,[35−37] and several MOFs.[18−20] Interestingly, encapsulation of RuBpy into zeolites or MOF materials has a significant impact on the photophysical properties of the complex. For example, encapsulation of RuBpy into the MOF USF2 resulted in a material in which the ^{3}MLCT lifetime was significantly extended relative to the complex in solution ($\tau_{Ethanol}$ = 614 ns and τ_{USF2} = 1.2 μs at 25 °C).[19] The extended lifetime was attributed to deactivation of a nonradiative ^{3}dd that is antibonding with respect to the RuBpy due to a confined molecular environment. Similar observations have been made for RuBpy complexes encapsulated within the cavities of zeolite Y, in which the size of the cavity completely deactivates the nonradiative ^{3}dd state.[29]

The presence of ionic species during synthesis of MOFs can also significantly influence the topology and charge of the resulting framework. For example, Burrows et al. reported on the influence of dimethylformamide (DMF) and diethylformamide (DEF) hydrolysis products on the framework formed with Zn(II) ions and benzene-1,4-dicarboxylate (bdc) ligands.[38] In the absence of water, the solvothermal reaction produces the well-known MOF-5 topology. However, addition of small amounts of water results in hydrolysis of the DMF or DEF, producing a $NH_2Et_2^+$ which templates formation of a new framework of the type $[NH_2Et_2]Zn_3(\mu\text{-bdc})_4]\cdot 2.5$ DEF. More recently, Zhang et al. utilized cationic porphyrins as templating agents to construct several new MOF frameworks that incorporate porphyrin-containing octahemioctahedral cavities.[11] These new MOFs contained crystallographically resolvable porphyrin macrocycles as well as catalytic activity toward hydrogen peroxide degradation. Although the RuBpy complex has yet to be explored as a templating agent, there is clear precedent for synthesis of new MOF topologies in the presence of the RuBpy cation with unique photophysical properties.

Here, synthesis of two new MOF frameworks formed from Zn(II) ions and 1,3,5-tris(4-carboxyphenyl)benzene templated by RuBpy is reported. Each structure contains crystallographically resolvable RuBpy clusters that exhibit photophysical properties consistent with encapsulation within a restricted environment. These new materials may serve as tunable platforms for development of a wide variety of Ru(II)(L)$_3$-encapsulated MOF frameworks using a RuBpy templating strategy.

METHODS

Synthesis of Zn/BTB *dia*, RWLC-1, and RWLC-2. Zn/BTB *dia* (parent MOF with no guest) was synthesized by adapting the MOF-39 procedure.[39,40] The Zn/BTB *dia* MOF was prepared by adding 1,3,5-tris(4-carboxyphenyl)benzene (H_3BTB) (15.4 mg, 0.035 mmol) to 3 mL of 1:1 (v/v) ethanol/dimethyformamide (EtOH/DMF) solution and $Zn(NO_3)_2\cdot 6H_2O$ (40.2 mg, 0.135 mmol) to 0.5 mL of H_2O. Solutions were mixed well in a scintillation vial and heated at 105 °C for 12 h. Crystals were removed and washed repeatedly with ethanol. Approximately 50−100 mg of crystals were recovered from the solution. RWLC-1 and RWLC-2 were synthesized by the procedure above but adding RuBpy (80 mg, 0.093 mmol for the Cl^- salt or 0.125 mmol for the PF_6^- salt) to the solution prior to heating. In the absence of RuBpy, neither RWLC-1 nor RWLC-2 was produced; rather, synthesis yielded the Zn/BTB *dia* structure.[39] The total yield of crystals was similar to that obtained for the Zn/BTB *dia* material. In the presence of RuBpy, both RWLC-1 and RWLC-2 structures appeared in the same reaction vial and were separated by hand under a microscope for crystallographic and spectroscopic analysis. Crystals were easily distinguishable as RWLC-1 crystals were rods emanating from a single point while RWLC-2 crystals were plate-like (Figure 1).

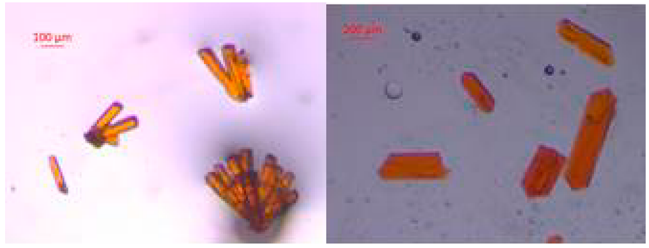

Figure 1. Microscopic images of RWLC-1 (left) and RWLC-2 (right). Images were obtained from a Zeiss SteREO Discovery V8Microscope with an Achromat S 1.0× FWD 63 mm objective and 2× or 1.25× zoom. Microscope is equipped with a Digital Microscopy CMOS Camera AxioCam ERc 5s, 1×.

Although the nature of the RuBpy counterion (PF_6^- or Cl^-) did not alter the structure of either RWLC-1 or RWLC-2, the distribution of RWLC-1 and RWLC-2 crystals in the reaction vial depended upon counterion with PF_6^- favoring RWLC-2 (~2:1 in crystal formation) while Cl^- favored RWLC-1 by the same proportion.

Steady-State and Time-Resolved Emission. Crystals of each material were immobilized on a glass slide with a thin layer of vacuum grease and placed into a cuvette containing a small amount of ethanol to prevent the crystals from drying. The cuvette was then deaerated with Ar gas. Steady-state emission and polarization measurements were performed using an ISS PC1 spectrofluorimeter. Emission was measured 45° relative to the 450 nm excitation beam. Polarization values were an average of 30 individual measurements. Lifetime measurements were performed on the same cuvette in a variable-temperature sample holder by excitation with a 7 ns laser pulse (fwhm) from a frequency-doubled Continuum MiniLite II frequency-doubled Nd:YAG laser (~1 mJ/pulse). Sample emission was collected 45° relative to the excitation beam with a focusing optic into an amplified Si-photodiode (EOT, ~200 ps rise time) and digitized using a 4 GHz transient digitizer (Tektronix 7404). Collected data is analyzed with OriginPro8.

X-ray Crystallography. X-ray diffraction data for RWLC-1 were collected using synchrotron radiation, λ = 0.41328 Å, at the Advanced Photon Source, Argonne National Lab, Chicago IL. X-ray diffraction data for RWLC-2 were collected using a Bruker-AXS SMART-APEXII CCD diffractometer (Cu Kα, λ = 1.54178 Å). Data have been processed using APEX2 software.[41] Structures have been solved using SHELXS-97 (direct methods) and refined using SHELXL-97.[42]

All non-H atoms have been located in the difference Fourier map. In both cases RuBpy was disordered. RuBpy has been freely refined in the RWLC-1 structure and is disordered over two positions with an occupancy ratio of 0.93:0.07. In RWLC-2, RuBpy is disordered over six positions in the channel and restraints have been used to obtain a chemically feasible model of the Bpy ligands. Significantly high electron density peaks corresponding to Ru allowed for determination of the Bpy ligand C and N atom locations. Detailed discussion can be found in the Supporting Information.

RESULTS AND DISCUSSION

MOF Structure. Structures of both RWLC-1 and RWLC-2 are shown in Figure 2 with the individual cavities displayed in Figure 3. In the structure of RWLC-1, two RuBpy cations, separated by PF_6^- (or Cl^-, RuBpy counterions), are confined within the large cavity surrounded by the framework formed by BTB ligands linking Zn_2OH clusters (Figure 4). The structure can be regarded as chains of Zn_2OH clusters, along the [001] direction, connected alternatively by carboxylate groups of the BTB ligand and hydrogen bonds between the OH^- and the

dx.doi.org/10.1021/ic402614w | Inorg. Chem. 2014, 53, 160−166

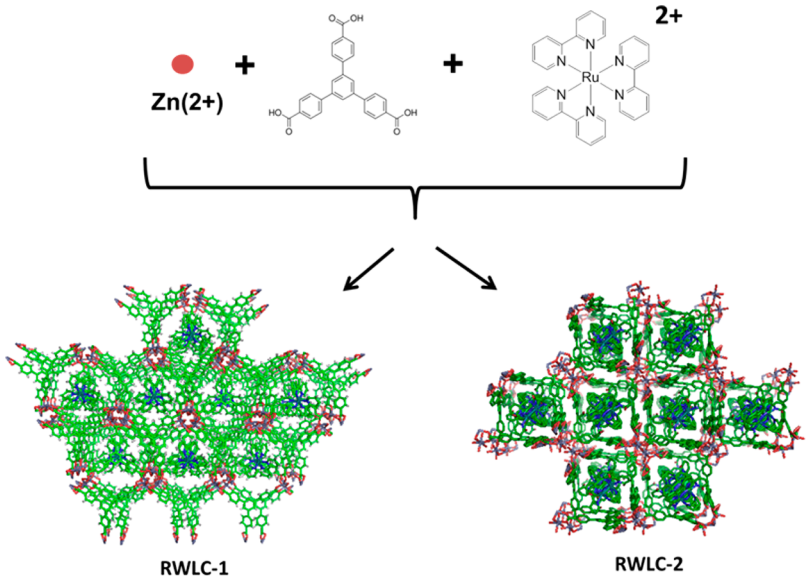

Figure 2. Overview of the structures formed by reaction of Zn^{2+} cations with BTB and RuBpy cations.

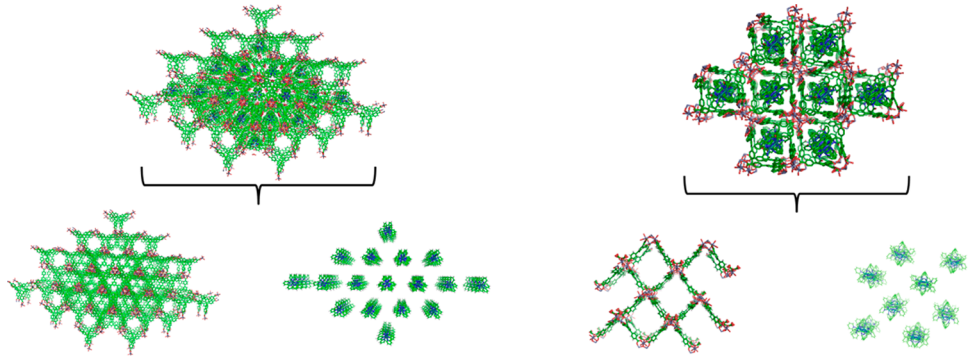

Figure 3. Crystal structures of RWLC-1 (left) and RWLC-2 (right) together with structural representations of the frameworks in which RuBpy was computationally separated from the framework to illustrate RuBpy alignment.

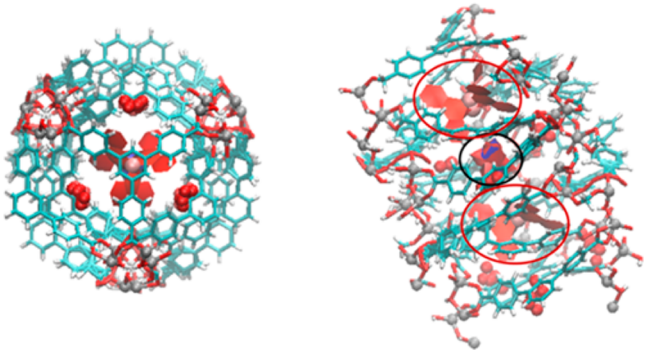

Figure 4. Diagram illustrating the cavities containing the RuBpy cations in RWLC-1. View on the left is down the long axis of the cavity, and view on the right is a side view. Black circle is the position of the PF_6^- ion, and orange circles are the RuBpy cations.

carboxylate groups. The hexagonal channels are blocked by BTB ligands forming cavities with two encapsulated RuBpy cations separated by a PF_6^- (or Cl^-) anion. The structure can still be considered a MOF as all clusters and ligands form a continuous network. The structure of RWLC-2 can be described as a 3,6-connected net with BTB ligands and Zn_3OH cluster (consisting of three Zn cations bridged by four carboxylates and an OH^- group in the center and other two carboxylates coordinated in a monodentate fashion) at corresponding vertices (Figure 5). The structure is similar to

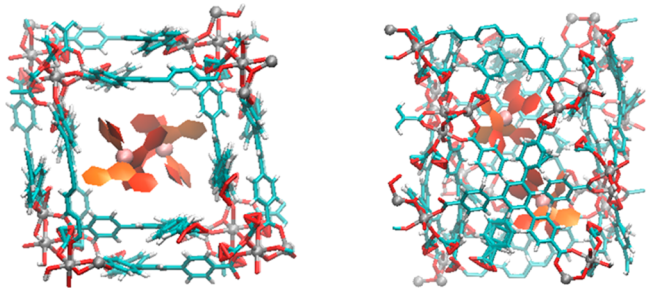

Figure 5. Diagram illustrating the cavities containing the RuBpy cations in RWLC-2. View on the left is down the long axis of the cavity, and view on the right is a side view.

that of the MOF-39 structure published by Yaghi and co-workers[40] with small changes to the cell parameters, related possibly to the presence of encapsulated RuBpy in the channels along the [100] direction.

Steady-State Emission. Steady-state emission spectra of the RuBpy encapsulated within RWLC-1 and RWLC-2 relative

dx.doi.org/10.1021/ic402614w | *Inorg. Chem.* 2014, 53, 160−166

to RuBpy in ethanol (solvent of intermediate polarity) are displayed in Figure 6. RWLC-1 exhibits a hypsochromic shift

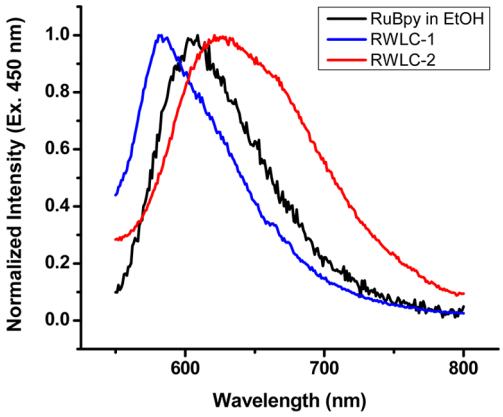

Figure 6. Normalized steady-state emission spectra of RuBpy in solution (black), RWLC-1 (blue), and RWLC-2 (red). Excitation wavelength was 450 nm.

relative to that of the RuBpy in ethanol (583 nm for RWLC-1 versus 606 nm for RuBpy in ethanol, Table 1). A similar

Table 1. Photophysical Parameters from Steady-State Luminescence Measurements

compound	λ_{max}, nm	polarization
RuBpy in EtOH	606	0.005 ± 0.002
RWLC-1	583	0.26 ± 0.03
RWLC-2	626	0.49 ± 0.04

hypsochromic shift has also been reported for RuBpy encapsulated within zeolite Y that has been dehydrated by heating the encapsulated material (586 nm for RuBpy@ZeoliteY versus ~626 nm for RuBpy in water).[29−32] Interestingly, in the hydrated RuBpy@ZeoliteY the emission spectrum of RuBpy was bathochromically shifted by nearly 11 nm. Shifts in the RuBpy emission maxima due to solvation changes arise from solvent interactions with the large dipole moment created upon excitation to the ^{3}MLCT. This dipole moment results in significant solvent reorganization, facilitating relaxation of the Franck−Condon excited state to the thermally relaxed ^{1}MLCT and intersystem crossing to the thermally relaxed ^{3}MLCT emissive state. In addition, hydrogen-bonding interactions between solvent molecules and the charge-separated Rubpy complex also contribute to the stability of the ^{3}MLCT. In the case of RuBpy confined within a solvent-restricted environment (e.g., dehydrated zeolite Y), solvent reorganization and hydrogen bonding are restricted, limiting thermal relaxation of the Franck−Condon ^{1}MLCT state, and emission arises from an unrelaxed ^{3}MLCT state, giving rise to hypsochromically shifted emission spectra relative to polar solvents. Examination of the crystal structure of RWLC-1 reveals two RuBpy cations separated by PF_6^- that make a very close fit with the framework with no resolvable solvent molecules in close proximity to the RuBpy clusters, similar to the dehydrated RuBpy@ZeoliteY material. As RWLC-1 is synthesized in a mixture of EtOH, DMF, and H_2O the presence of polar/hydrogen-bonding H_2O/EtOH molecules within the cavities would result in a less hypsochromically shifted spectrum.

In contrast to RWLC-1, the emission spectrum for RWLC-2 exhibits a large bathochromic shift relative to RuBpy in solution (626 nm for RWLC-2 versus 606 nm for RuBpy in ethanol), consistent with the presence of H_2O molecules within the framework channels. Should EtOH molecules be present the emission maximum would resemble that of the solution spectrum (in EtOH). A bathochromic shift relative to EtOH arises from a relaxed ^{3}MLCT state with further stabilization due to solvent interactions. Unlike the RWLC-1 structure, the RuBpy complexes observed within the channels of RWLC-2 are located ~9 Å apart, providing gaps for solvent occupancy that are in close enough in proximity to participate in intermolecular interactions with neighboring RuBpy clusters, leading to enhanced stabilization of the ^{3}MLCT state. Indeed, refinement of structural models based upon single-crystal X-ray diffraction data reveals several electron density peaks that can be interpreted as disordered water molecules in close vicinity of RuBpy.

Interestingly, emission spectra of RWLC-1 and RWLC-2 are both distinct from that observed for the RuBpy@USF2 material previously reported.[19] The spectrum of RuBpy@USF2 displays only a slight hypsochromic shift relative to that of RuBpy in solution (604 nm for RuBpy in EtOH versus 598 nm for RuBpy in USF2), indicating the presence of EtOH molecules within the cavities.[19] Unlike the two new materials, RuBpy cations

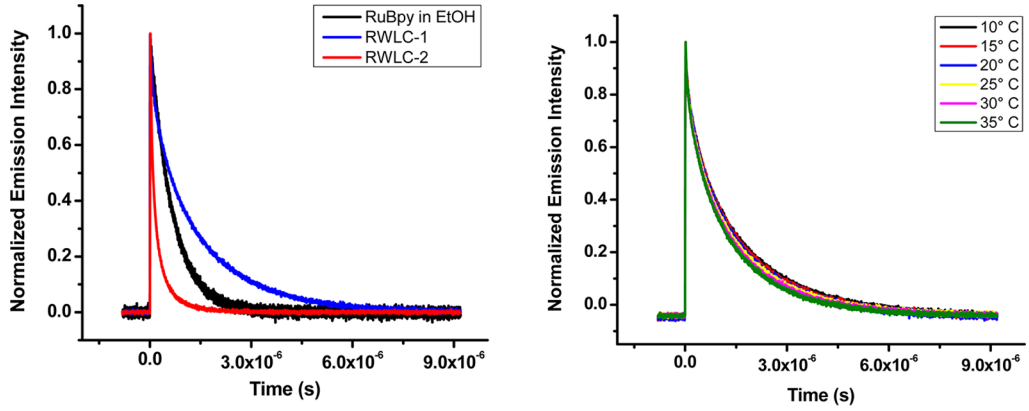

Figure 7. (Left) Normalized time-resolved emission decays of RuBpy in solution (black), RWLC-1 (blue), and RWLC-2 (red) at 25 °C. Excitation wavelength was 532 nm. (Right) Overlay of normalized time-resolved emission decays of RWLC-1 depicting temperature dependence. Spectra were fit to biexponential functions.

dx.doi.org/10.1021/ic402614w | Inorg. Chem. 2014, 53, 160−166

cannot be crystallographically resolved in the USF2 material (composed of Zn(II) and benzene tricarboxylate ligands).

Time-Resolved Emission. Figure 7, left, displays an overlay of the normalized emission decays of RuBpy in EtOH, RWLC-1, and RWLC-2 at 25 °C under anaerobic conditions. RuBpy in EtOH exhibits a single-exponential decay with a lifetime of 676 ns, while the RWLC-1 and RWLC-2 materials exhibit emission decays that are best fit to a biexponential function. The best-fit lifetimes and amplitudes for each MOF are listed in Table 2. The slow phase lifetimes

Table 2. Photophysical Parameters from Time-Resolved Emission Measurements

compound	k_0, $s^{-1} \times 10^5$	k_1, $s^{-1} \times 10^{11}$	ΔE_1, cm^{-1}	τ, ns
RuBpy in EtOH	5.6	191	3491	676
RWLC-1-fast	38.3	267	3753	237
RWLC-1-slow	5.3	0.2	2566	1600
RWLC-2-fast	39.8	125	3256	171
RWLC-2-slow	7.6	0.2	2198	797
RuBpy@USF2[a]	5.64	514	4593	1200
RuBpy@ZeoliteY[b]	3.8	0.0011	890	530

[a]Data from ref 19. [b]Data from ref 29.

associated with RWLC-1 (1.60 μs, 72% of the total amplitude) and RWLC-2 (797 ns, 72% of the total amplitude) are significantly longer than RuBpy in solution (676 ns), while the observed fast phase lifetimes are significantly shorter (237 ns, 28% of the total amplitude and 171 ns, 28% of the total amplitude for RWLC-1 and RWLC-2, respectively).

Excited-state decay processes for RuBpy are summarized in the energy level diagram outlined in Figure 8, left.[43,44] The diagram illustrates both radiative and nonradiative pathways from the ^{3}MLCT to the ground state as well as a nonradiative ligand field decay channel (^{3}dd). The observed emission decay rate constant is expressed as

$$k_{obs} = k_0 + k_1 \exp(-\Delta E_1/RT) \quad (1)$$

where k_{obs} is $1/\tau_{obs}$, $k_0 = k_r + k_{nr}$, k_r and k_{nr} are the radiative and nonradiative ^{3}MLCT decay rate constants, respectively, k_1 is the nonradiative decay rate constant from the ^{3}dd state, and ΔE_1 is the energy gap between the ^{3}MLCT state and the ^{3}dd state. Examining the emission decay lifetimes as a function of temperature (Figure 7, right) allows for determination of k_0, k_1, and ΔE_1 for the RWLC-1 and RWLC-2 complexes, and these results are summarized in Figure 9, and the resulting constants are summarized in Table 2.

The ΔE_1 value for the 1.60 μs decay of RWLC-1 is 2566 cm^{-1} and for the 797 ns phase of RWLC-2 is 2198 cm^{-1}, both of which are significantly lower than the solution value (3491 cm^{-1}). In addition, the corresponding k_1 values are 3 orders of magnitude smaller than that observed for RuBpy in EtOH (2×10^{10} versus 1.91×10^{13} s^{-1}, respectively). It has been previously observed that for RuBpy confined to zeolite Y cavities the ΔE_1 value for the ^{3}dd state increases well above the solution value such that nonradiative deactivation through the ^{3}dd channel is no longer accessible.[29] The ^{3}dd state is dissociative with regard to the Ru−L bonds, resulting in an expansion of the RuBpy complex, which cannot take place within a sufficiently small cavity (Figure 8, right). Alternatively, the 890 cm^{-1} ΔE_1 value observed for RuBpy encapsulated in zeolite Y was assigned to a fourth ^{3}MLCT state which lies slightly above the ^{3}MLCT manifold. The rate constant for the decay of the fourth ^{3}MLCT is on the order of 10^8, which restricts the observed decay lifetime to approximately 530 ns. Interestingly, previous studies have shown that the USF2 material exhibits an increase in the ΔE_1 to 4593 cm^{-1} with a corresponding lifetime of 1.2 μs.[19] This ΔE_1 value lies between that of RuBpy encapsulated in zeolite Y cavities and RuBpy in solution (for the energy difference between the ^{3}dd and the ^{3}MLCT) and was also attributed to a restricted expansion.

ΔE_1 values for RWLC-1 and RWLC-2 preclude involvement of the ^{3}dd nonradiate decay channel as a reduction in this energy would result in a significantly enhanced decay rate (much shorter observed lifetime) relative to that observed in solution. Alternatively, these values are much higher than would be expected for the energy gap between the three-state ^{3}MLCT manifold and the fourth ^{3}MLCT state (890 cm^{-1}). An interesting possibility is that the RuBpy encapsulated within the RWLC-1 and RWLC-2 materials accesses MLCT states higher in energy than the fourth MLCT state (Figure 8, right). Computational studies have determined that two additional singlet in character MLCT states lie higher in energy than the fourth ^{3}MLCT states by 2450 and 3100 cm^{-1}, similar to the ΔE_1 values determined for RWLC-1 and RWLC-2.[45] These states have been observed experimentally at 2442 and 3096 cm^{-1} above the fourth MLCT state in single crystals of $RuBpy(ClO_4)_2$.[46] The state at 2442 cm^{-1} has tentatively been assigned as a ^{1}dπ^* state. Although the decay rates for this state have not been previously reported, the k_1 values observed here (2×10^{10} s^{-1}) are consistent with nonradiative decay.

The corresponding fast phase observed in both RWLC-1 and RWLC-2 (accounting for 28% of the total intensity in both materials) exhibits photophysical properties distinct from those observed for the slower phases. Examination of the k_0, k_1, and ΔE_1 values indicate that the ^{3}dd decay is nearly identical to that of RuBpy in solution with the exception of the k_0 values (k_0 of 3.83×10^6, 3.98×10^6, and 5.6×10^5 s^{-1}; k_1 of 2.67×10^{13}, 1.25×10^{13}, and 1.91×10^{13} s^{-1}; ΔE_1 of 3753, 3256, and 3491 cm^{-1} for RWLC-1, RWLC-2, and RuBpy in ethanol, respectively). The fact that the ΔE_1 and k_1 values are nearly identical to those observed for RuBpy in ethanol indicates that this population of RuBpy is located in a less constrained environment in both materials. However, examination of the crystal structures does not reveal additional cavities other than the highly constrained cavities/channels with resolvable RuBpy complexes, suggesting that the fast phase population exists in nonperiodic or defect regions within the crystal. A number of studies have appeared that characterize such nonperiodic regions in MOF crystals including HKUST-1 and MOF-5.[47,48] The data further reveal that the RuBpy complexes within nonperiodic regions are also quenched relative to the specifically encapsulated RuBpy or RuBpy in solution as determined from the k_0 values, which are an order of magnitude larger than solution values. As the k_0

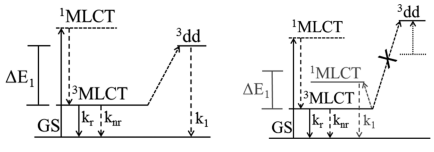

Figure 8. RuBpy excited state decay pathways. (Left) RuBpy in ethanol. (Right) Proposed population of a ^{1}MLCT and associated decay pathway of RuBpy in RWLC-1 and RWLC-2.[43,44] Solid lines represent radiative decay pathways, while dashed lines represent nonradiative decay pathways.

dx.doi.org/10.1021/ic402614w | Inorg. Chem. 2014, 53, 160−166

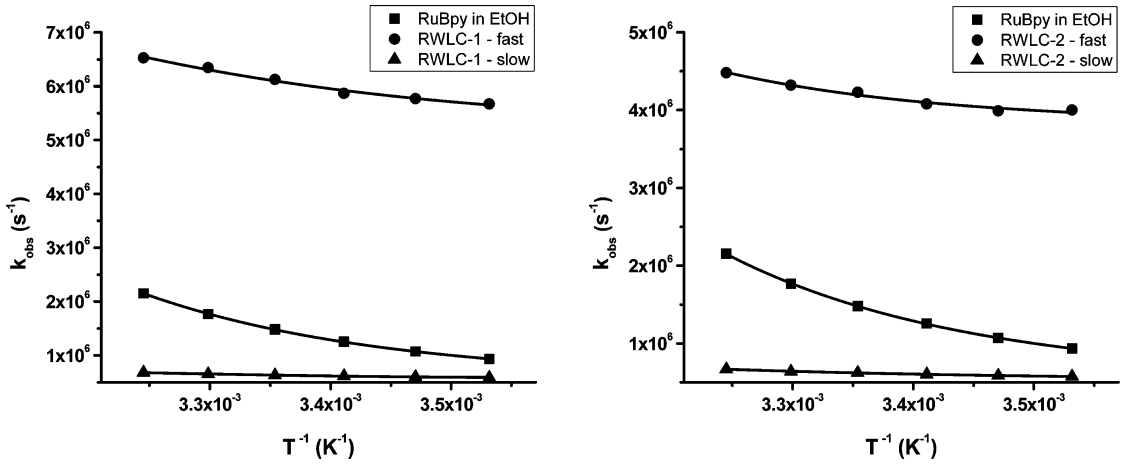

Figure 9. Fits of the observed rate constants versus $1/T$ for RuBpy decay in solution and both phases of RWLC-1 (left) and RWLC-2 (right).

values reflect decay from the ^{3}MLCT state the quenching mechanism most likely reflects either energy or electron transfer between the excited RuBpy complexes and a coentrapped quencher. DMF easily hydrolyzes to diethylamine (DEA) at elevated temperatures and in the presence of water. As DEA is an effective quencher of the RuBpy ^{3}MLCT, it is quite possible that the short lifetime components of RWLC-1 and RWLC-2 are due to coencapsulation of RuBpy and DEA into larger nonperiodic regions of the crystal. Attempts to remove the putative quencher(s) through extensive washing were unsuccessful, indicating that the larger, nonperiodic regions may not be accessible to the bulk solvent.

It is also noteworthy that the slow phase lifetime for RWLC-1 is roughly twice that of RWLC-2 as well as a ΔE_1 that is ~400 cm^{-1} higher but with the same k_1 values. Examination of the crystal structures of the two materials reveals a cavity with no solvent in close proximity to RuBpy for RWLC-1, while the RWLC-2 material contains solvent molecules within the cavities. The slow phase data would indicate that the ^{1}MLCT state is somewhat influenced by solvent reorganization. The corresponding fast phase lifetimes are also distinct between RWLC-1 and RWLC-2, with RWLC-1 (237 ns, ΔE_1 = 3753 cm^{-1}) longer than RWLC-2 (171 ns, ΔE_1 = 3256 cm^{-1}). Though this ^{3}dd decay lifetime in both MOFs is attributed to RuBpy in a nonperiodic region with a coencapsulated quencher, additional solvent molecules likely reduce the energy of the ^{3}dd state in RWLC-2.

SUMMARY

Data presented here demonstrates the ability of RuBpy cations to template new MOFs and the ability to tune existing frameworks. Both structures contain crystallographically resolvable RuBpy clusters encapsulated within the cavities and channels. The photophysical properties are consistent with RuBpy cations in two distinct environments that modulate the excited-state properties. Specifically, encapsulation in the very confined cavities of RWLC-1 and RWLC-2 completely deactivates the ligand field state (^{3}dd), while a rarely observed ^{1}MLCT decay channel becomes active. The second population appears to be located in nonperiodic regions within the MOF crystals that have relatively large cavities and coencapsulate a quencher, likely DEA (hydrolysis product of DMF) formed during MOF synthesis.

ASSOCIATED CONTENT

Supporting Information

X-ray crystallographic data for RWLC-1 and RWLC-2 in cif format and single crystal X-ray diffraction details. This material is available free of charge via the Internet at http://pubs.acs.org.

AUTHOR INFORMATION

Corresponding Author

*E-mail: rlarsen@cas.usf.edu.

Notes

The authors declare no competing financial interest.

ACKNOWLEDGMENTS

Crystal diffraction of RWLC-1 MOF was carried out at the Advanced Photon Source on beam line 15ID-C of ChemMatCARS Sector 15, which is principally supported by the National Science Foundation/Department of Energy under grant no. NSF/CHE-0822838. Use of the Advanced Photon Source was supported by the U.S. Department of Energy, Office of Science, Office of Basic Energy Sciences, under contract no. DE-AC02-06CH11357. Part of this work was also supported by the Department of Defense–Defense Threat Reduction Agency (DoD-DTRA) through HDTRA1-08-C-0035.

REFERENCES

(1) Cheetham, A. K.; Ferey, G.; Loiseau, T. *Angew. Chem., Int. Ed.* **1999**, *38*, 3268–3292.
(2) Zaworotko, M. J. *Nature* **1999**, *402*, 242–243.
(3) Eddaoudi, M.; Moler, D. B.; Li, H.; Chen, B.; Reineke, T. M.; O'Keeffe, M.; Yaghi, O. M. *Acc. Chem. Res.* **2001**, *34*, 319–330.
(4) Tanabe, K. K.; Cohen, S. M. *Chem. Soc. Rev.* **2011**, *40*, 498–519.
(5) Stock, N.; Biswas, S. *Chem. Rev.* **2012**, *112*, 933–969.
(6) Cook, T. R.; Zheng, Y.-R.; Stang, P. J. *Chem. Rev.* **2013**, *113*, 734–777.
(7) Lu, J.; Mondal, A.; Moulton, B.; Zaworotko, M. J. *Angew. Chem., Int. Ed.* **2001**, *40*, 2113–2116.
(8) Alkordi, M. H.; Liu, Y.; Larsen, R. W.; Eubank, J. F.; Eddaoudi, M. *J. Am. Chem. Soc.* **2008**, *130*, 12639–12641.
(9) Larsen, R. W.; Wojtas, L.; Perman, J.; Musselman, R. L.; Zaworotko, M. J.; Vetromile, C. M. *J. Am. Chem. Soc.* **2011**, *133*, 10356–10359.
(10) Larsen, R. W.; Miksovska, J.; Musselman, R. L.; Wojtas, L. *J. Phys. Chem. A* **2011**, *115*, 11519–11524.
(11) Zhang, Z.; Zhang, L.; Wojtas, L.; Nugent, P.; Eddaoudi, M.; Zaworotko, M. J. *J. Am. Chem. Soc.* **2012**, *134*, 928–933.

(12) Song, J.; Luo, Z.; Britt, D. K.; Furukawa, H.; Yaghi, O. M.; Hardcastle, K. I.; Hill, C. L. *J. Am. Chem. Soc.* **2011**, *133*, 16839−16846.
(13) Wee, L. H.; Wiktor, C.; Turner, S.; Vanderlinden, W.; Janssens, N.; Bajpe, S. R.; Houthoofd, K.; Van Tendeloo, G.; De Feyter, S.; Kirschhock, C. E. A.; Martens, J. A. *J. Am. Chem. Soc.* **2012**, *134*, 10911−10919.
(14) Zheng, S.-T.; Yang, G.-Y. *Dalton Trans.* **2010**, *39*, 700−703.
(15) Juan-Alcañiz, J.; Ramos-Fernandez, E. V.; Lafont, U.; Gascon, J.; Kapteijn, F. *J. Catal.* **2010**, *269*, 229−241.
(16) Liu, X.; Wang, L.; Yin, X.; Huang, R. *Eur. J. Inorg. Chem.* **2013**, *19*, 2181−2187.
(17) Paes De Sousa, P.; Grazina, R.; Barbosa, A. D. S.; De Castro, B.; Moura, J. J. G.; Cunha-Silva, L.; Balula, S. S. *Electrochim. Acta* **2013**, *87*, 853−859.
(18) Sen, R.; Koner, S.; Bhattacharjee, A.; Kusz, J.; Miyashita, Y.; Okamoto, K.-I. *Dalton Trans.* **2011**, *40*, 6952−6960.
(19) Larsen, R. W.; Wojtas, L. *J. Phys. Chem. A* **2012**, *116*, 7830−7835.
(20) Pointillart, F.; Train, C.; Gruselle, M.; Villain, F.; Schmalle, H. W.; Talbot, D.; Gredin, P.; Decurtins, S.; Verdaguer, M. *Chem. Mater.* **2004**, *16*, 832−841.
(21) Cai, B.; Ren, Y.; Jiang, H.; Zheng, D.; Shi, D.; Qian, Y.; Hu, H. *Inorg. Chem. Commun.* **2012**, *15*, 159−162.
(22) Decurtins, S.; Schmalle, H. W.; Schneuwly, P.; Ensling, J.; Gütlich, P. *J. Am. Chem. Soc.* **1994**, *116*, 9521−9528.
(23) Sieber, R.; Decurtins, S.; Stoeckli-Evans, H.; Wilson, C.; Yufit, D.; Howard, J. A. K.; Capelli, S. C.; Hauser, A. *Eur. J. Chem.* **2000**, *6*, 361−368.
(24) Andres, R.; Gruselle, M.; Malezieux, B.; Verdaguer, M.; Vaissermann, J. *Inorg. Chem.* **1999**, *38*, 4637−4646.
(25) Pointillart, F.; Train, C.; Boubekeur, K.; Gruselle, M.; Verdaguer, M. *Tetrahedron: Asymmetry* **2006**, *17*, 1937−1943.
(26) Pellaux, R.; Decurtins, S.; Schmalle, H. W. *Acta Crystallogr.* **1999**, *C55*, 1075−1079.
(27) Andres, R.; Brissard, M.; Gruselle, M.; Train, C.; Vaissermann, J.; Malezieux, B.; Jamet, J. P.; Verdaguer, M. *Inorg. Chem.* **2001**, *40*, 4633−4640.
(28) Balzani, V.; Juris, A.; Serroni, S. *Chem. Rev.* **1996**, *96*, 759−833.
(29) Maruszewski, K.; Strommen, D. P.; Kincaid, J. R. *J. Am. Chem. Soc.* **1993**, *115*, 8345.
(30) Incavo, J. A.; Dutta, P. K. *J. Phys. Chem.* **1990**, *94*, 3075−3081.
(31) Lainé, P.; Lanz, M.; Calzaferri, G. *Inorg. Chem.* **1996**, *35*, 3514−3518.
(32) Sykora, M.; Kincaid, J. R.; Dutta, P. K.; Castagnola, N. B. *J. Phys. Chem. B* **1999**, *103*, 309−320.
(33) Kumar, C. V.; Williams, Z. J. *J. Phys. Chem.* **1995**, *99*, 17632−17639.
(34) Martí, A. A.; Colón, J. L. *Inorg. Chem.* **2010**, *49*, 7298−7303.
(35) Matsui, K.; Momose, F. *Chem. Mater.* **1997**, *9*, 2588−2591.
(36) Ma, D.; Bettis, S. E.; Hanson, K.; Minakova, M.; Alibabaei, L.; Fondrie, W.; Ryan, D. M.; Papoian, G. A.; Meyer, T. J.; Waters, M. L.; Papanikolas, J. M. *J. Am. Chem. Soc.* **2013**, *135*, 5250−5253.
(37) Maruszewski, K.; Jasiorski, M.; Salamon, M.; Stręk, W. *Chem. Phys. Lett.* **1999**, *314*, 83−90.
(38) Burrows, A. D.; Cassar, K.; Friend, R. M. W.; Mahon, M. F.; Rigby, S. P.; Warren, J. E. *CrystEngComm* **2005**, *7*, 548−550.
(39) Caskey, S. R.; Wong-Foy, A. G.; Matzger, A. J. *Inorg. Chem.* **2008**, *47*, 7751−7756.
(40) Kim, J.; Chen, B.; Reineke, T. M.; Li, H.; Eddaoudi, M.; Moler, D. B.; O'Keeffe, M.; Yaghi, O. M. *J. Am. Chem. Soc.* **2001**, *123*, 8239−824742.
(41) *APEX2*; Bruker-AXS Inc.: Madison, WI, 2010.
(42) Sheldrick, G. M. *Acta Crystallogr.* **2008**, *A64*, 112−122.
(43) Crosby, G. A.; Perkins, W. G.; Klassen, D. M. *J. Chem. Phys.* **1965**, *43*, 1498−1503.
(44) Durham, B.; Caspar, J. V.; Nagle, J. K.; Meyer, T. J. *J. Am. Chem. Soc.* **1982**, *104*, 4803−4810.
(45) Heully, J.-L.; Alary, F.; Boggio-Pasqua, M. *J. Chem. Phys.* **2009**, *131*, 184308−1−9.
(46) Komada, Y.; Yamauchi, S.; Hirota, N. *J. Phys. Chem.* **1988**, *92*, 6511−6518.
(47) Qiu, L.-G.; Xu, T.; Li, Z.-Q.; Wang, W.; Wu, Y.; Jiang, X.; Tian, X.-Y.; Zhang, L.-D. *Angew. Chem., Int. Ed.* **2008**, *47*, 9487−9491.
(48) Xin, Z.; Bai, J.; Pan, Y.; Zaworotko, M. J. *Chem.—Eur. J.* **2010**, *16*, 13049−13052.